Photo-switchable pure water splitting under visible light over nano-Pt@P25 by recycling scattered photons

Wenjian Fang, Zhen Qin, Junying Liu, Zhidong Wei, Zhi Jiang, Wenfeng Shangguan*

Research Centre for Combustion and Environment Technology, Shanghai Jiao Tong University, Shanghai, 200240, PR China

ABSTRACT

Visible light absorption peak from near-field dielectric scattering was observed in case of Pt nanoparticles directly supported on P25. This absorbed scattered light could drive visible-light photocatalytic pure water splitting ($\lambda > 420$ nm). It is interesting that the roles of Pt and P25 in photocatalytic hydrogen generation were switchable under different irradiation conditions. Under UV–vis irradiation, P25 represented a photocatalyst while Pt was cocatalyst. Under visible light irradiation ($\lambda > 420$ nm), Pt would prefer to act as a photocatalyst while P25 was analogous to cocatalyst. Moreover, defects (Ti^{3+} or V_O) on the surface of Pt/P25 would be generated under UV irradiation. These defects are similar with a sacrificial agent to consume photogenerated holes, which are necessary for visible-light-drive photocatalytic pure water splitting.

1. Introduction

Since the discovery of the Honda-Fujishima effect in 1972, photocatalysis has been applied to solve energy and environmental problems which attracts much attention all over the world [1]. Generally, photocatalysts are almost exclusively semiconductors which can harvest solar energy to decompose water and eliminate contaminants [2–7]. To date, kinds of semiconductor photocatalysts have been reported to be able to split water. Among them, TiO_2, CdS and g-C_3N_4 etc. have been under an extensive research [8–13]. On the other hand, metal nanoparticles also have the ability to harvest solar energy through the interaction of free electrons in metals with photons [14–16]. Tian et al. first discovered that surface plasmon resonance (SPR) induced by metals has potential application to photocatalysis [17]. It is demonstrated that energetic electron can drive directly photocatalysis on plasmonic metallic nanostructures and induce enhancements in the rates of photocatalytic water splitting on composite Plasmonic-metal/semiconductor photocatalysts. For example, by incorporating Au or Ag nanoparticles into semiconductors (such as TiO_2, g-C_3N_4 and CdS), hot electrons excited on SPR states of Au or Ag will inject to the conduction band of semiconductors [14,18–20].

However, observable SPR peaks from Pt nanoparticles (< 10 nm) have never been reported before [21,22]. Recently, Zhang et al. proposed a new light absorption model to modulate the absorption peak of supported small Pt nanoparticles, which exhibit well-defined visible-light absorption peaks and can drive photocatalytic redox reactions [23,24]. However, these specific optical absorption peaks of small Pt

nanoparticles are especially sensitive to the support and synthesis method. For example, this absorption from near-field dielectric scattering cannot be observed in case of Pt nanoparticles directly supported on TiO_2.

As we know, Pt nanoparticles (< 10 nm), supported on various semiconductor photocatalysts, are also an excellent cocatalyst for the hydrogen evolution reaction [25–27]. The photoexcited electrons can rapidly transfer from semiconductors to the Pt nanoparticles to reduce H_2O. However, Pt as cocatalyst is usually thought to be adverse for pure water splitting because hydrogen back-oxidation may also be catalyzed by Pt nanoparticles. Recently, it is reported that Pt nanoparticles in a higher oxidation state can act as an efficient hydrogen evolution cocatalyst without back reaction [28,29].

Above all, Pt nanoparticles may play a switchable role, harvesting solar energy as photocatalyst and promoting hydrogen evolution as cocatalyst. Especially, it has been reported that TiO_2 supported with small Pt nanoparticles can promote visible-light-driven photocatalytic redox processes [21,23,30]. There is an intriguing question to be explored that what caused this visible light absorption. It was analyzed that both Pt nanoparticles and defected TiO_2 may result in visible light absorption. Shiraishi et al. reported that visible light irradiation ($\lambda > 450$ nm) of Pt nanoparticles supported on anatase TiO_2 promotes efficient aerobic oxidation at room temperature [30]. Zhai et al. also found that Pt nanoparticles supported on anatase TiO_2 can drive selective oxidation of aromatic alcohols to aldehydes in water under visible light irradiation at ambient temperature [21]. Meanwhile, Naldoni et al. found that the bandgap narrowing is dictated by the

---
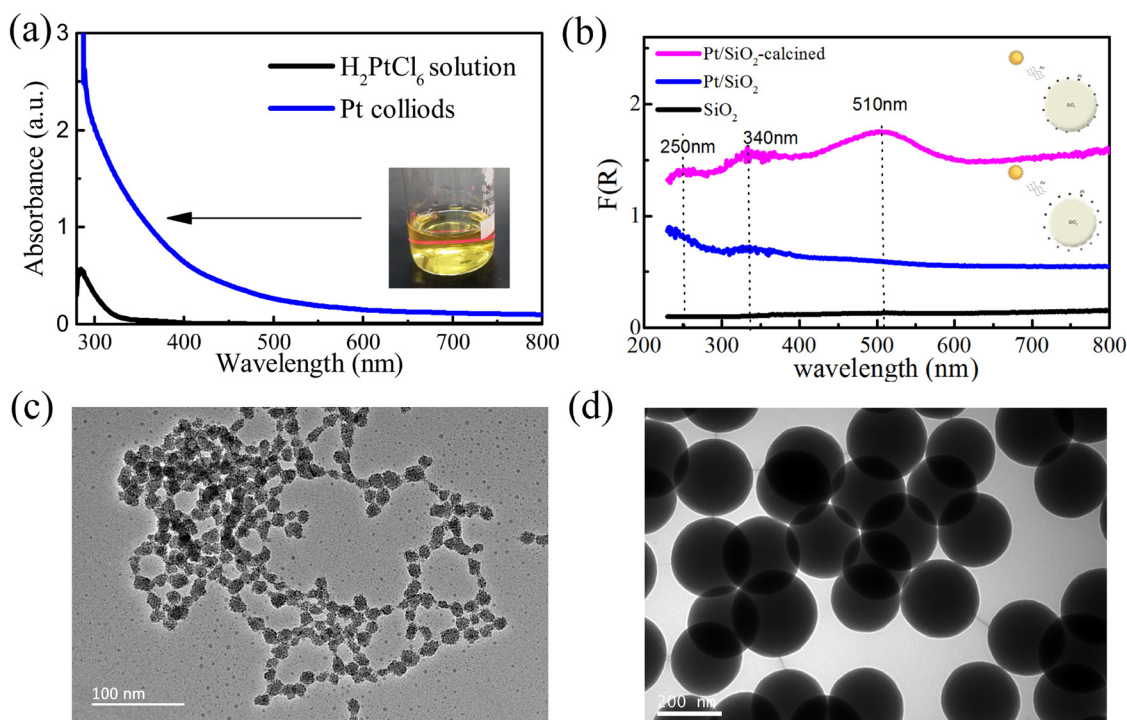
Fig. 1. (a) UV–vis absorption spectrum of stabilized Pt colloids (Insets: photograph of Pt colloids); (b) UV–vis DRS spectrum of SiO$_2$ spheres, Pt/SiO$_2$ and Pt/SiO$_2$-calcined plotted as the Kubelka-Munk function of the reflectance R; (c) TEM image of Pt nanoparticles; (d) TEM image of SiO$_2$ spheres.

synergistic presence of V$_O$'s and surface disorder [31]. However, the oxygen vacancy and Ti^{3+} defects would lower the position of the conduction band of TiO$_2$ [32]. Thus, the photocatalytic activity in generating hydrogen would decrease.

Though TiO$_2$ with Pt nanoparticles as cocatalyst has shown photocatalytic activity under visible light, there were few reports about visible-light water splitting conducted by Pt/TiO$_2$. Therefore, photocatalytic hydrogen generation under visible light (λ > 420 nm) by P25 with Pt nanoparticles as cocatalyst would be shown in this paper. The origination of this visible-light-driven photocatalytic activity was analyzed. Moreover, the relation between photocatalytic hydrogen generation and light waveband was proposed for the first time.

2. Experiment

2.1. Chemicals

Aeroxide P25 were purchased from Evonik without further modification. Others reagents were purchased from Sinopharm Chemical Reagent Co., Ltd., (China). Ultrapure water was used throughout this work. All other reagents were of analytical reagent grade, without further purification.

2.2. Preparation of Pt colloids

H$_2$PtCl$_6$ solution containing 4 mg Pt was added to the 80 mL ultrapure water. The suspension was vigorous stirring in dark with a continuous flow of Ar for 30 min. when the suspension was well mixed and the air was expelled, it was then thoroughly degassed and irradiated by Xe lamp for 2 h. After that, the yellow Pt colloids was obtained.

2.3. Preparation of Pt/SiO$_2$

SiO$_2$ spheres were prepared via the Stöber method. A typical procedure is as follows. Firstly, 10 mL of deionized H$_2$O and 3 mL of NH$_3$·H$_2$O was injected respectively into a mixture of 75 mL of ethyl

alcohol at room temperature under magnetic stirring for 30 min. Then, 6 mL of TEOS was added slowly to the solution above. After reacting for 6 h, the colloidal spheres were collected by centrifugation and washed with ultrapure water for several times. Then, the sediment was dried in an electronic oven at 353 K. Then, 0.2 g SiO$_2$ as prepared was suspended in 80 mL ultrapure water with ultrasound for 20 min in a Pyrex reaction cell. In situ photo-deposition Pt was followed as preparation of Pt colloids above. After that, the yellow sediment Pt/SiO$_2$ was filtered and dried at 353 K in air for overnight. Finally, the Pt/SiO$_2$ was calcined in air at 623 K for 2 h, named as Pt/SiO$_2$-calcined.

2.4. Preparation of Pt/P25

In situ photo-deposition Pt on P25 was also followed as above. The only different is that it is irradiated by Xe lamp only for 20 min. After that, the dusty blue sediment Pt/P25 was filtered and dried at 353 K in air for overnight.

2.5. Photocatalytic reaction for water splitting

The photocatalytic reactions were carried out in a Pyrex reaction cell connected to a closed gas circulation and evacuation system. Typically, 0.1 g Pt/P25 was suspended in 80 mL ultrapure water. Then the suspension was thoroughly degassed and irradiated by a Xe lamp (300 W). The amount of H$_2$ and O$_2$ were analysed every hour using an online gas chromatography. When performing a reaction under visible light (the UV–vis transmittance of cutoff filter was shown in Fig. S1), the reaction vessel was completely shielded from any light by aluminium foil (excluding the top of the vessel).

2.6. Characterizations

The UV–vis diffuse reflection spectra (DRS) were determined by a UV–vis spectrophotometer UV-2450 (Shimadzu, Japan) and were converted to absorbance by the Kulbelka-Munk method. The morphology of the products was investigated by transmission electronic micrograph

(TEM, JEM-2010, operated at 200 kV). The XPS patterns were measured on an AXIS UltraDLD electronic energy spectrum (Kratos group) at 300 W using Mg Kα X-rays as the excitation source. The binding energies (B.E.) of the elements were calibrated relative to the carbon impurity with a C 1 s at 284.8 eV. Raman spectra were recorded on a Raman spectrometer (Jasco NRS-2100), in which a laser of 532 nm was used as an excitation source.

3. Results and discussion

We first found that an aqueous dispersion of stabilized Pt nanoparticles can be obtained by in situ photo-deposition H_2PtCl_6 solutions as shown in Fig. 1(a). The Pt colloids show yellow color with obvious Tindall effect. However, it exhibits broadband optical absorption with no distinct absorption peak from the ultraviolet to the visible-light region. From Fig. 1(c), the size of Pt nanoparticles mainly has two distributions (~3 nm and ~10 nm). It is found that Pt nanoparticles with large size are agglomerated by Pt nanoparticles with about 3 nm. Thus, we speculate that the size of Pt nanoparticles can be controlled by light intensity and light frequency. Interestingly, this aqueous dispersion of stabilized Pt nanoparticles cannot be obtained by in situ photo-deposition H_2PtCl_6 solution with sacrificial agent (such as methyl alcohol).

Based on previous reference [23], the Pt nanoparticles were loaded onto SiO_2 by in situ photo-deposition H_2PtCl_6 solution method. From the UV–vis DRS spectrum of Pt/SiO_2-calcined as shown in Fig. 1(b), three distinct absorption peaks located at ~250, 340 and 510 nm were observed. Such recognizable absorption peaks could not be detected in either the pristine SiO_2 spheres or Pt/SiO_2 without calcined. So, we concluded that such small Pt nanoparticles integrated with SiO_2 tightly would promote a new optical absorption. However, it was frustrating that this optical absorption of Pt/SiO_2-calcined nearly has no ability to drive visible-light-driven water splitting. Though hot electrons can be excited by Pt nanoparticles, SiO_2 is an inert material that has no photocatalytic activity. To be capable of utilizing this absorbed visible light for hydrogen generation, supports have better be changed to semiconductor photocatalysts. Among them, P25 might be suitable which is almost transparent in visible light ($\lambda > 400$ nm).

Therefore, the Pt nanoparticles are loaded onto P25 using in situ photo-deposition H_2PtCl_6 solution method as well. From Fig. 2, Pt nanoparticles with ~3 nm are dispersed uniformly on the surface of P25. Moreover, the size of P25 is nonuniformity changing from 30 nm to 100 nm. To avoid Pt nanoparticles agglomerated, the in situ photo-deposition time should not be too long. In our experiment, the photodeposition time was 20 min. It is worth mentioning that the color of Pt/
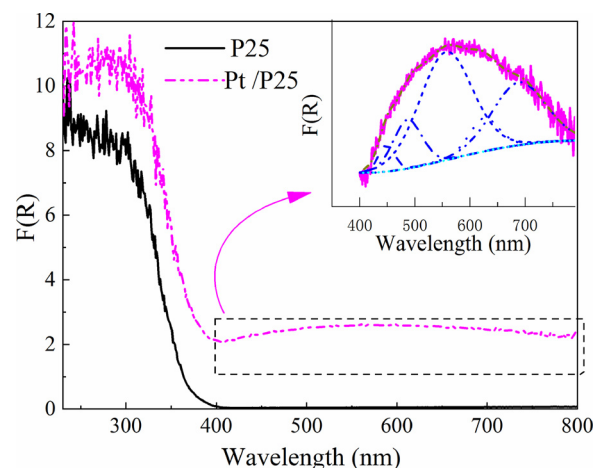

Fig. 3. UV–vis DRS spectrum of P25 and Pt/P25. (Inset: a narrow range).

P25 solution is dusty blue.

Furthermore, the optical properties of Pt/P25 were investigated by UV–vis DRS spectrum. From the Fig. 3, the absorption intensity of Pt/P25 is enhanced from UV to visible light compared with P25. It is extremely encouraging that a broad absorption peak from 400 nm to 800 nm can be distinguished easily. According to previous studies, there are three possible reasons for the enhanced visible light absorption: metallicity of Pt nanoparticles, defects of P25 and the absorption of scattered light in the near field. However, metallicity of Pt nanoparticles and defects of P25 cannot result in observable peaks [33,34]. Thus, we think this broad absorption peak is mainly contributed by the absorption of scattered light in the near field. From the Fig. 3(inset), this broad absorption peak can be fitted well by some small peaks. It has been reported that with an increase in the diameter of the supports, a redshift of the scattering and absorption peaks of Pt/supports occurs [23]. So the broad absorption peak is mainly due to the different sizes and irregular morphology of P25.

Next, visible-light-driven pure water splitting by Pt colloids, Pt/SiO_2-calcined and Pt/P25 were performed. The spectrum of the Xe lamp and the reflection spectrum of the cutoff filter ($\lambda > 420$ nm) are given in Fig. S1. There is no suspense that few H_2 was detected with Pt colloids or Pt/SiO_2-calcined as photocatalysts under UV–vis irradiation. However, in comparison, the photocatalytic activity of Pt/P25 has some interesting and ambiguous phenomena as shown in Figs. 4 and 5. Firstly, during the process of in situ photo-deposition Pt, the production of H_2 and O_2 are 30 μmol and 316 μmol respectively. It is puzzling that
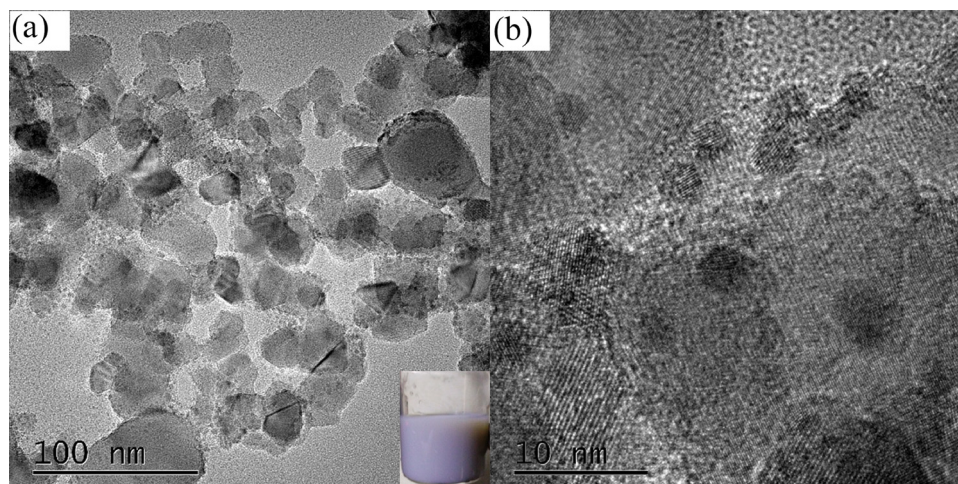
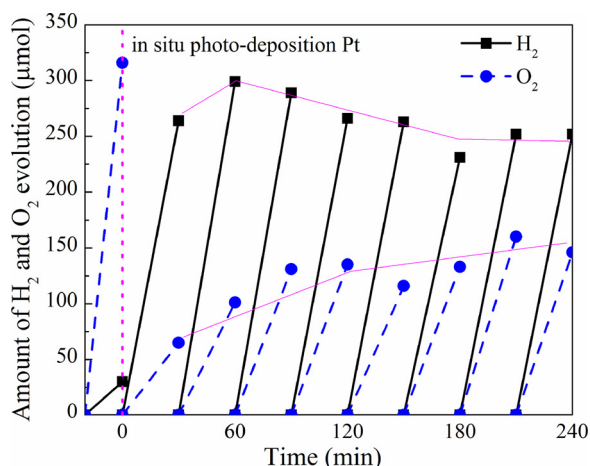

Fig. 2. HRTEM image of Pt/P25 nanoparticles.

Fig. 4. The photocatalytic activity of Pt/P25 under Xe lamp without a cutoff filter.

the amount of O_2 is too larger to satisfied charge balance. Except photo-induced electron was used to reduce H_2O to H_2 ($\sim 40\,\mu mol$) and Pt^{4+} to Pt^0 ($\sim 10\,\mu mol$), where were the remainder photo-induced electron? Secondly, during the procedure of pure water splitting by Pt/P25, it is found that the amount of H_2 and O_2 productivity were not instability. The production rates of H_2 has a declining trend, while O_2 has an opposite trend. Thirdly, this decreased photocatalytic hydrogen generation activity can be restored after only visible light irradiation ($\lambda > 420\,nm$) or black reaction (see Fig. 5).

On the other hand, through the test of visible-light photocatalytic activity of Pt/P25, it is found that no gases are produced directly under visible light irradiation ($\lambda > 420\,nm$) at the very first. Then without cutoff filter irradiation for half an hour, it is exciting that H_2 is continually generated with average production rates $\sim 5\,\mu mol/h$ ($\lambda > 420\,nm$). However, the O_2 is not detected. Furthermore, O_2 might be consumed away if O_2 was injected into the reaction cell artificially.

From the results above, we think the mechanism of photocatalytic hydrogen generation under UV ($\lambda < 400\,nm$) and visible light ($\lambda > 420\,nm$) by P25 with Pt nanoparticles as cocatalyst is different. From the Fig. 3, it is obviously that P25 itself cannot absorb the visible light ($\lambda > 400\,nm$). Here, visible-light-driven photocatalytic activity induced by defects of P25 is excluded firstly. It has been reported that the energy level of localized donor states originating from oxygen

vacancies is located at $0.75 \sim 1.18\,eV$ below the conduction band of P25, which is lower than the redox potential of H^+/H_2 (0 V vs. NHE) [10]. Therefore, visible-light absorption caused by defects states of P25 is adverse for photocatalytic hydrogen generation. Therefore, the origination of this visible-light-driven photocatalytic activity might be connected with Pt nanoparticles, which can absorb scattered light in the near field of the dielectric surface of the P25. However, the facts are not such simple as this visible-light photocatalytic activity of Pt/P25 need to be activated by UV ($\lambda < 400\,nm$). Thus, it is speculated that something of Pt/P25 should be changed under UV–vis irradiation. Raman and XPS were further used to explore the exact changes of Pt/P25 under UV–vis irradiation.

The Raman spectra of P25 and Pt/P25 are given in Fig. 6(a), which is very sensitive to the crystallinity and microstructure of materials. The Raman active modes of P25 are mainly ascribed to anatase (E_g modes: 141.5, 196, and $636.5\,cm^{-1}$; B_{1g} modes: $394\,cm^{-1}$ and $516\,cm^{-1}$; A_{1g} modes: $394\,cm^{-1}$). It is found that the strongest intensity mode around $141\,cm^{-1}$ is broadened slightly and blue-shift after in situ photo-deposition Pt. while the peaks at $516\,cm^{-1}$ and $636.5\,cm^{-1}$ were shifted to shorter wavenumbers. This phenomenon has also been observed in TiO_2 supported with graphite-like carbon layers, which indicate that a close interaction might exist between Pt and P25 [35,36]. On the other hand, defects of P25 can also result in Raman band shifting and changes of peak width [32]. So, high-resolution XPS was used to detect the chemical bonding of the surface elements. The binding energies (B.E.) of the elements were calibrated relative to the carbon impurity with a C 1s at 284.8 eV. From the high-resolution Pt 4f, Pt/P25 photocatalyst has two obvious peaks of Pt 4f7/2 and Pt 4f5/2 at 70.6 and 74.4 eV, respectively, indicating the existence of the metallic Pt [28]. From the high-resolution O 1s and Ti 2p, two changes are meaningful and noteworthy. One is peak shift of Ti 2p3/2 (from 458.4 to 458.6 eV) and O 1s (from 529.6 to 529.8 eV) toward high energy after in situ photo-deposition Pt, which indicates the formation of oxygen vacancies. The other is the appearance of low-energy shoulder (456.8 eV) in the Ti 2p spectrum, which is the characteristic feature for Ti^{3+} ions [37,38]. On the basis of previous studies, oxygen vacancies in TiO_2 can be formed by high-temperature heating and/or ultra-high vacuum, high-energy particle bombardment, ion sputtering, γ-ray or ultraviolet (UV) irradiation [39]. Especially, low-energy UV photons (3.4 and 4.7 eV) could produce Ti^{3+} surface defects which were stable in a vacuum but could be healed by O_2 exposure [40]. Moreover, photoinduced defects would be accelerated in aqueous methanol solutions [41]. Therefore, it is concluded that defects (Ti^{3+} or V_O) on the surface of Pt/P25 would be produced
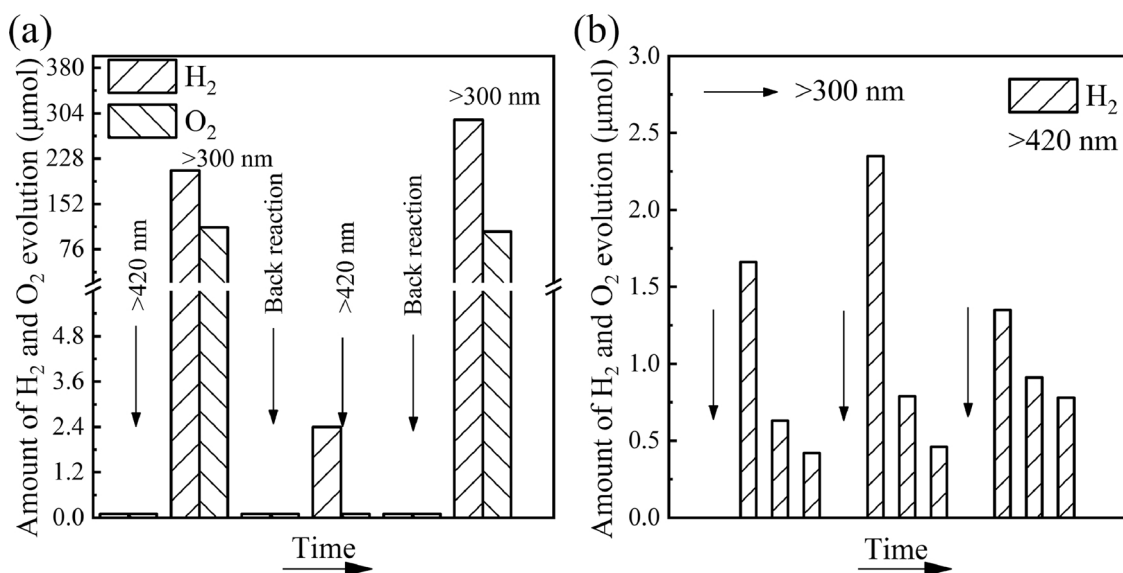

Fig. 5. The photocatalytic activity of Pt/P25 under Xe lamp with cutoff filter (every break time 0.5 h). The UV–vis transmittance of cutoff filter was shown in Fig. S1.
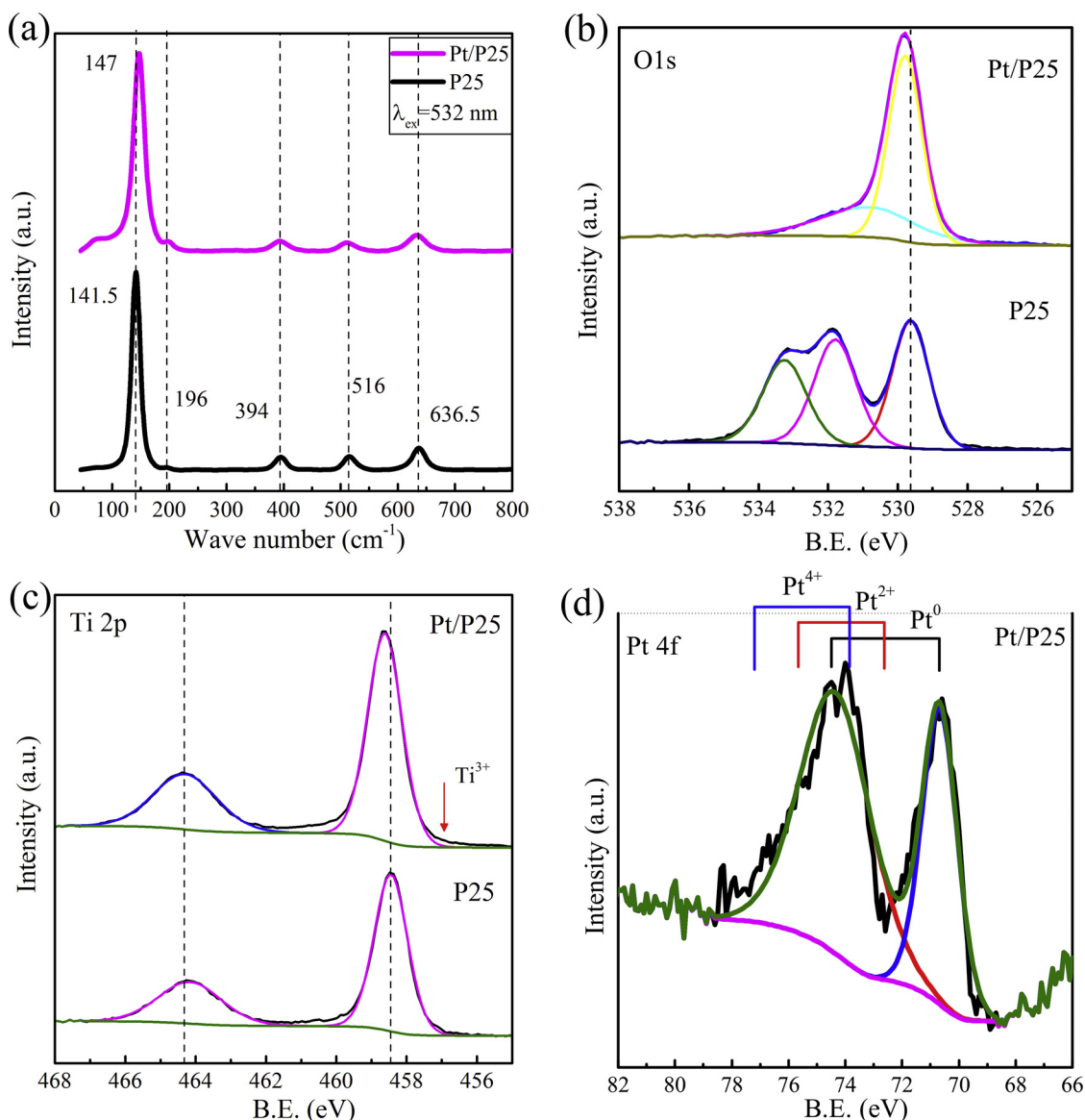
Fig. 6. XPS survey spectra and Raman spectra of P25 and Pt/P25.

under UV irradiation. The close interaction between Pt and P25 might promote photo-induced defects. Moreover, there were any significant changes for P25 itself under UV irradiation in pure water.

The mechanism of photocatalytic hydrogen generation under UV–vis ($\lambda > 300$ nm) and visible light ($\lambda > 420$ nm) by P25 with Pt nanoparticles as cocatalyst are illustrated in Fig. 7. If Pt/P25 irradiated under UV light, the energy of incident light is larger enough to generate electrons and holes in the conduction and valence band of P25, respectively. Then, photogenerated electrons will reduce H_2O to form H_2 while photogenerated holes oxidize H_2O to form O_2. In particular, the reducibility of these photogenerated electrons is too strong to reduce Ti^{4+} to Ti^{3+} under vacuum conditions. So, defects of Pt/P25 will appear during the photocatalytic reaction for water splitting. As we know, impurity energy introduced by these defects is adverse for photocatalytic hydrogen generation. Therefore, it is observed that photocatalytic reaction for water splitting was not instability (see Fig. 4). Due to the consumption photogenerated electrons to reduce Ti^{4+}, the production rates of H_2 has a declining trend. If Pt/P25 irradiated visible light irradiation ($\lambda > 420$ nm), the energy of incident light cannot generate electrons and holes in the conduction and valence band of P25. At this time, photogenerated electrons and holes are mainly

induced in the metal Pt nanoparticles, which can absorb scattered light in the near field of the dielectric surface of the P25. The energetic hot electrons can transfer to the conduction band of P25 and reduce H_2O to form H_2 [42]. The photogenerated holes located below Fermi level of Pt can move to the surface of P25 via the "tunneling" manner and drive photocatalytic redox processes. As the oxidization of H_2O to O_2 is hard and restrict, photogenerated holes prefer to oxidized Ti^{3+} to Ti^{4+} during the photocatalytic reaction under visible light irradiation ($\lambda > 420$ nm) (see Fig. 5). Recently, oxygen vacancies in ultrafine Bi_5O_7Br nanotubes has been proved to take part in the reaction of solar-driven nitrogen fixation in Pure Water [43]. Thus, defects existed on the surface of P25 is a necessity. The role of defects is similar with a sacrificial agent, which is used to consume photogenerated holes. So the visible-light photocatalytic activity of Pt/P25 need to be activated by UV–vis light irradiation.

4. Conclusion

An aqueous dispersion of stabilized Pt nanoparticles was obtained by in situ photo-deposition H_2PtCl_6 solution. Based on this method, the Pt nanoparticles are loaded onto SiO_2 sphere which shows three distinct
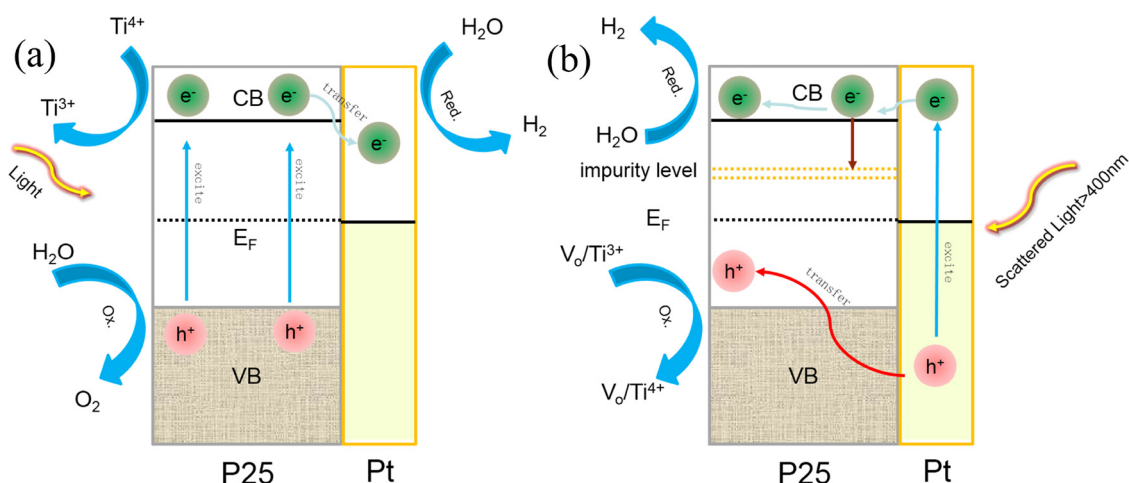
Fig. 7. Schematic illustration for charge carriers transfer in the Pt/P25 composites under UV–vis light irradiation (a) and visible light irradiation (b).

absorption peaks located at ∼250, 340 and 510 nm in the UV–vis DRS spectrum. Furthermore, the Pt nanoparticles are loaded onto P25 using in situ photo-deposition H_2PtCl_6 solution method as well. This Pt/P25 shows a broad absorption peak from 400 nm to 800 nm. This broad absorption peak is thought to be contributed by the absorption of scattered light in the near field of P25, which can be fitted well by some small peaks. Visible-light-driven pure water splitting by Pt/P25 was performed that H_2 is continually generated with average production rates ∼5 μmol/h ($\lambda > 420$ nm). The mechanism of photocatalytic hydrogen generation under UV–vis ($\lambda > 300$ nm) and visible light ($\lambda > 420$ nm) by P25 with Pt nanoparticles as cocatalyst are illustrated. Under UV irradiation, P25 is photocatalyst while Pt is cocatalyst. Under visible light ($\lambda > 420$ nm), Pt is photocatalyst while P25 is analogous to cocatalyst. It is meaningful about this switchable role in photocatalytic water splitting.

Acknowledgments

Appendix A. Supplementary data

Supplementary material related to this article can be found, in the online version, at doi:https://doi.org/10.1016/j.apcatb.2018.05.023.

References

[1] A. Fujishima, K. Honda, Electrochemical photolysis of water at a semiconductor electrode, Nature 238 (1972) 37–38.
[2] H. Tong, S. Ouyang, Y. Bi, N. Umezawa, M. Oshikiri, J. Ye, Nano-photocatalytic materials: possibilities and challenges, Adv. Mater. 24 (2012) 229–251.
[3] H. Wang, L. Zhang, Z. Chen, J. Hu, S. Li, Z. Wang, J. Liu, X. Wang, Semiconductor heterojunction photocatalysts: design, construction, and photocatalytic performances, Chem. Soc. Rev. 43 (2014) 5234–5244.
[4] X. Chen, S. Shen, L. Guo, S.S. Mao, Semiconductor-based photocatalytic hydrogen generation, Chem. Rev. 110 (2010) 6503–6570.
[5] A. Kudo, Y. Miseki, Heterogeneous photocatalyst materials for water splitting, Chem. Soc. Rev. 38 (2009) 253–278.
[6] S. Chen, T. Takata, K. Domen, Particulate photocatalysts for overall water splitting, Nat. Rev. Mater. 2 (2017) 17050.
[7] X.F. Qian, D.T. Yue, Z.Y. Tian, M. Reng, Y. Zhu, M. Kan, T.Y. Zhang, Y.X. Zhao, Carbon quantum dots decorated Bi_2WO_6 nanocomposite with enhanced photo-catalytic oxidation activity for VOCs, Appl. Catal. B: Environ. 193 (2016) 16–21.
[8] H.G. Yang, C.H. Sun, S.Z. Qiao, J. Zou, G. Liu, S.C. Smith, H.M. Cheng, G.Q. Lu, Anatase TiO_2 single crystals with a large percentage of reactive facets, Nature 453 (2008) 638–641.
[9] Z. Wang, C. Yang, T. Lin, H. Yin, P. Chen, D. Wan, F. Xu, F. Huang, J. Lin, X. Xie, M. Jiang, H-doped black titania with very high solar absorption and excellent photocatalysis enhanced by localized surface plasmon resonance, Adv. Funct.

Mater. 23 (2013) 5444–5450.
[10] H. Song, C. Li, Z. Lou, Z. Ye, L. Zhu, Effective formation of oxygen vacancies in black tio_2 nanostructures with efficient solar-driven water splitting, ACS Sustain. Chem. Eng. 5 (2017) 8982–8987.
[11] X. Chen, W. Chen, H. Gao, Y. Yang, W. Shangguan, In situ photodeposition of NiO_X on CdS for hydrogen production under visible light: enhanced activity by controlling solution environment, Appl. Catal. B: Environ. 152–153 (2014) 68–72.
[12] J. Liu, Y. Liu, N. Liu, Y. Han, X. Zhang, H. Huang, Y. Lifshitz, S.T. Lee, J. Zhong, Z. Kang, Water splitting. Metal-free efficient photocatalyst for stable visible water splitting via a two-electron pathway, Science 347 (2015) 970–974.
[13] R. Asahi, T. Morikawa, T. Ohwaki, K. Aoki, Y. Taga, Visible-light photocatalysis in nitrogen-doped titanium oxides, Science 293 (2001) 269–271.
[14] S. Linic, P. Christopher, D.B. Ingram, Plasmonic-metal nanostructures for efficient conversion of solar to chemical energy, Nat. Mater. 10 (2011) 911–921.
[15] M. Pagliaro, Recycling scattered light for energy conversion, Mater. Today 20 (2017) 49–50.
[16] D. Mateo, I. Esteve-Adell, J. Albero, J.F. Royo, A. Primo, H. Garcia, {111} oriented gold nanoplatelets on multilayer graphene as visible light photocatalyst for overall water splitting, Nat. Commun. 7 (2016) 11819.
[17] Y. Tian, T. Tatsuma, Mechanisms and applications of plasmon-induced charge separation at TiO_2 films loaded with gold nanoparticles, J. Am. Chem. Soc. 127 (2005) 7632–7637.
[18] J. Xue, S. Ma, Y. Zhou, Z. Zhang, M. He, Facile photochemical synthesis of Au/Pt/g-C_3N_4 with plasmon-enhanced photocatalytic activity for antibiotic degradation, ACS Appl. Mater. Interface 7 (2015) 9630–9637.
[19] D.B. Ingram, S. Linic, Water splitting on composite plasmonic-metal/semiconductor photoelectrodes: evidence for selective plasmon-induced formation of charge carriers near the semiconductor surface, J. Am. Chem. Soc. 133 (2011) 5202–5205.
[20] E. Thimsen, F. Le Formal, M. Gratzel, S.C. Warren, Influence of plasmonic Au nanoparticles on the photoactivity of Fe_2O_3 electrodes for water splitting, Nano Lett. 11 (2011) 35–43.
[21] W. Zhai, S. Xue, A. Zhu, Y. Luo, Y. Tian, Plasmon-driven selective oxidation of aromatic alcohols to aldehydes in water with recyclable Pt/TiO_2 nanocomposites, ChemCatChem 3 (2011) 127–130.
[22] N.C. Bigall, T. Hartling, M. Klose, P. Simon, L.M. Eng, A. Eychmuller, Monodisperse platinum nanospheres with adjustable diameters from 10 to 100 nm: synthesis and distinct optical properties, Nano Lett. 8 (2008) 4588–4592.
[23] N. Zhang, C. Han, Y.-J. Xu, J.J. Foley IV, D. Zhang, J. Codrington, S.K. Gray, Y. Sun, Near-field dielectric scattering promotes optical absorption by platinum nanoparticles, Nat. Photon. 10 (2016) 473–482.
[24] K.D. Rasamani, J.J. Foley IV, B. Beidelman, Y. Sun, Enhanced optical absorption in semiconductor nanoparticles enabled by near-field dielectric scattering, Nano Res. 10 (2017) 1292–1301.
[25] K. Maeda, Photocatalytic properties of rutile TiO_2 powder for overall water splitting, Catal. Sci. Technol. 4 (2014) 1949–1953.
[26] Z. Jiang, Z. Zhang, W. Shangguan, M.A. Isaacs, L.J. Durndell, C.M.A. Parlett, A.F. Lee, Photodeposition as a facile route to tunable Pt photocatalysts for hydrogen production: on the role of methanol, Catal. Sci. Technol. 6 (2016) 81–88.
[27] J. Yu, L. Qi, M. Jaroniec, Hydrogen production by photocatalytic water splitting over Pt/TiO_2 nanosheets with exposed (001) facets, J. Phys. Chem. C 114 (2010) 13118–13125.
[28] Y.H. Li, J. Xing, Z.J. Chen, Z. Li, F. Tian, L.R. Zheng, H.F. Wang, P. Hu, H.J. Zhao, H.G. Yang, Unidirectional suppression of hydrogen oxidation on oxidized platinum clusters, Nat. Commun. 4 (2013) 2500.
[29] G. Zhang, Z.-A. Lan, L. Lin, S. Lin, X. Wang, Overall water splitting by Pt/g-C_3N_4 photocatalysts without using sacrificial agents, Chem. Sci. 7 (2016) 3062–3066.
[30] Y. Shiraishi, D. Tsukamoto, Y. Sugano, A. Shiro, S. Ichikawa, S. Tanaka, T. Hirai, Platinum nanoparticles supported on anatase titanium dioxide as highly active catalysts for aerobic oxidation under visible light irradiation, ACS Catal. 2 (2012) 1984–1992.

[31] A. Naldoni, M. Allieta, S. Santangelo, M. Marelli, F. Fabbri, S. Cappelli, C.L. Bianchi, R. Psaro, V. Dal Santo, Effect of nature and location of defects on bandgap narrowing in black TiO_2 nanoparticles, J. Am. Chem. Soc. 134 (2012) 7600–7603.

[32] J.C. Parker, R.W. Siegel, Raman microprobe study of nanophase TiO_2 and oxidation-induced spectral changes, J. Mater. Res. 5 (1990) 1246–1252.

[33] X. Pan, Y.J. Xu, Efficient thermal- and photocatalyst of Pd nanoparticles on TiO_2 achieved by an oxygen vacancies promoted synthesis strategy, ACS Appl. Mater. Interfaces 6 (2014) 1879–1886.

[34] X. Jiang, Y. Zhang, J. Jiang, Y. Rong, Y. Wang, Y. Wu, C. Pan, Characterization of oxygen vacancy associates within hydrogenated TiO_2: a positron annihilation study, J. Phys. Chem. C 116 (2012) 22619–22624.

[35] L.W. Zhang, H.B. Fu, Y.F. Zhu, Efficient TiO_2 photocatalysts from surface hybridization of TiO_2 particles with graphite-like carbon, Adv. Funct. Mater. 18 (2008) 2180–2189.

[36] K.D. Schierbaum, S. Fischer, M.C. Torquemada, J.L.D. Segovia, E. Román, J.A. Martín-Gago, The interaction of Pt with TiO_2 (110) surfaces: a comparative XPS, UPS, ISS, and ESD study, Surf. Sci. 345 (1996) 261–273.

[37] T. Xia, Y. Zhang, J. Murowchick, X. Chen, Vacuum-treated titanium dioxide nanocrystals: optical properties, surface disorder, oxygen vacancy, and photocatalytic activities, Catal. Today 225 (2014) 2–9.

[38] G. Liu, H.G. Yang, X. Wang, L. Cheng, H. Lu, L. Wang, G.Q. Lu, H.-M. Cheng, Enhanced photoactivity of oxygen-deficient anatase TiO_2 sheets with dominant {001} facets, J. Phys. Chem. C 113 (2009) 21784–21788.

[39] X. Pan, M.Q. Yang, X. Fu, N. Zhang, Y.J. Xu, Defective TiO_2 with oxygen vacancies: synthesis, properties and photocatalytic applications, Nanoscale 5 (2013) 3601–3614.

[40] A.N. Shultz, W. Jang, W.M.H. Iii, D.R. Baer, L.Q. Wang, M.H. Engelhard, Comparative second harmonic generation and x-ray photoelectron spectroscopy studies of the UV creation and O_2 healing of Ti^{3+} defects on (110) rutile TiO_2 surfaces, Surf. Sci. 339 (1995) 114–124.

[41] X. Yang, C. Salzmann, H. Shi, H. Wang, M.L. Green, T. Xiao, The role of photo-induced defects in TiO_2 and its effects on hydrogen evolution from aqueous methanol solution, J. Phys. Chem. A 112 (2008) 10784.

[42] P. Wang, T.F. Xie, H.Y. Li, L. Peng, Y. Zhang, T.S. Wu, S. Pang, Y.F. Zhao, D.J. Wang, Synthesis and plasmon-induced charge-transfer properties of monodisperse gold-doped titania microspheres, Chemistry 15 (2009) 4366–4372.

[43] S. Wang, X. Hai, X. Ding, K. Chang, Y. Xiang, X. Meng, Z. Yang, H. Chen, J. Ye, Light-switchable oxygen vacancies in ultrafine Bi_5O_7Br nanotubes for boosting solar-driven nitrogen fixation in pure water, Adv. Mater. 29 (2017) 1701774.